Inorganic Chemistry

Article

pubs.acs.org/IC

Photosensitization Behavior of Ir(III) Complexes in Selective Reduction of CO_2 by Re(I)-Complex-Anchored TiO_2 Hybrid Catalyst

Ha-Yeon Cheong, So-Yoen Kim, Yang-Jin Cho, Dae Won Cho, Chul Hoon Kim, Ho-Jin Son,* Chyongjin Pac,* and Sang Ook Kang*

Department of Advanced Materials Chemistry, Korea University, Sejong 30019, Korea

Supporting Information

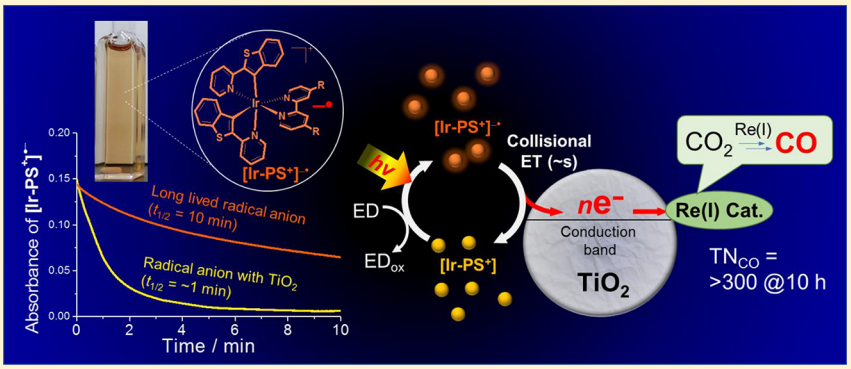

ABSTRACT: A series of cationic Ir(III) complexes ($[Ir(btp)_2(bpy\text{-}X_2)]^+$ (**Ir-X**$^+$: btp = (2-pyridyl)benzo[*b*]thiophen-3-yl; bpy-X_2 = 4,4′-X_2-2,2′-bipyridine (X = OMe, ^{t}Bu, Me, H, and CN)) were applied as visible-light photosensitizer to the CO_2 reduction to CO using a hybrid catalyst (TiO_2/ReP) prepared by anchoring of Re(4,4′-Y_2-bpy)$(CO)_3Cl$ (ReP; Y = $CH_2PO(OH)_2$) on TiO_2 particles. Irradiation of a solution containing **Ir-X**$^+$, TiO_2/ReP particles, and an electron donor (1,3-dimethyl-2-phenyl-1,3-dihydrobenzimidazole) in *N*,*N*-dimethylformamide at greater than 400 nm resulted in the reduction of CO_2 to CO with efficiencies in the order X = OMe > ^{t}Bu ≈ Me > H; **Ir-CN**$^+$ has no photosensitization effect. A notable observation is that **Ir-^{t}Bu**$^+$ and **Ir-Me**$^+$ are less efficient than **Ir-OMe**$^+$ at an early stage of the reaction but reveal persistent photosensitization behavior for a much longer period of time unlike the latter. Comparable experiments showed that (1) the **Ir-X**$^+$ sensitizers are commonly superior compared to $Ru(bpy)_3^{2+}$, a widely used transition-metal photosensitizer, and (2) the system comprising **Ir-OMe**$^+$ and TiO_2/ReP is much more efficient than a homogeneous-solution system using **Ir-OMe**$^+$ and Re(4,4′-Y'_2-bpy)$(CO)_3Cl$ (Y′ = $CH_2PO(OEt)_2$). Implications of the present observations involving reaction mechanisms associated with the different behavior of the photosensitizers are discussed in detail.

INTRODUCTION

Development of efficient catalytic systems for visible-light-induced CO_2 reductions has attracted great attention associated with the greenhouse effect due to the rapid increase of CO_2 concentration in the atmosphere by combustion of fossil fuels.[1−4] Building up such photocatalytic systems for CO_2 reductions requires optimum combination of a visible-light-absorbing antenna and a CO_2-reduction catalyst that can achieve an efficient visible-light-driven flow of electrons from an electron donor to the catalyst followed by multielectron reductions of CO_2. Among various catalysts used in visible-light reductions of CO_2, transition-metal complexes have been receiving much attention associated with their potentialities in high catalytic efficiencies and high chemical selectivity.[5−7] In particular, Re(I) complexes with a general formula of Re(L)$(CO)_3Y^{n+}$ (abbreviated as ReC; L = 2,2′-bipyridine or a related ligand, Y = auxiliary ligand, and *n* = 0 or 1) are attractive because of the remarkable capability in performing the efficient and selective reduction of CO_2 to CO,[8,9] being applied to versatile systems involving homogeneous-solution photosensitization[6,10−14] and heterogeneous dye sensitization[15−22] of the CO_2 reduction under visible-light irradiation.

Chart 1 illustrates typical reaction systems related to the present investigation on the application of ReC to the visible-light-induced reduction of CO_2 to CO; (a) homogeneous-solution photosensitization[10,13,14] that is typically initiated by electron transfer from an electron donor (ED) to a photosensitizer (PS) in the excited state followed by electron donation from the one-electron reduced species of PS ($PS^{-\bullet}$) to reduction catalyst (ReC), (b) a dye sensitization system[15,16,20−23] constructed by anchoring both PS (Dye) and ReC on semiconductor particles (typically TiO_2), in which electrons are injected into the semiconductor from excited-state PS and then transported to ReC, and (c) a mixed system comprising free PS and ReC-anchored semiconductor particles, which is relevant to the main subject of the present investigation.[24]

Received: August 14, 2017

DOI: 10.1021/acs.inorgchem.7b01963
Inorg. Chem. XXXX, XXX, XXX−XXX

Chart 1. Schematic Representation of Three Reaction Systems Related to the Present Investigation on the Photocatalytic Reduction of CO_2 to CO[a]

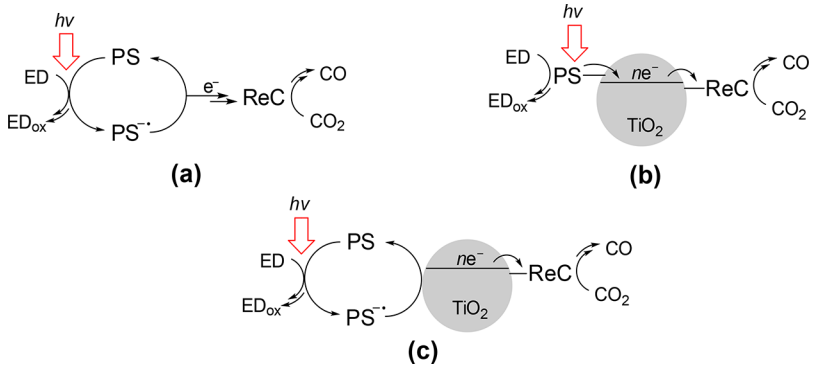

[a]ReC = Re(I) complex catalyst, PS = photosensitizer, and ED = electron donor; (a) homogeneous system, (b) ternary system, and (c) binary system.

Recently, we reported that a hybrid system[20−23] constructed by covalent anchoring of both a visible-light absorbing bithiophene (BT)-based dye (Dye) and ReC on TiO_2 particles (i.e., ternary system in Chart 1b, PS = Dye) reveals highly improved durability in the visible-light CO_2 reduction to CO; this system is abbreviated as Dye/TiO_2/ReC (Dye = Ar_2N-BT-CH═C(CN)COOH and ReC = ReP = Re(4,4′-Y_2-bpy)$(CO)_3Cl$ (Y = $CH_2PO(OH)_2$)). The photocatalytic CO_2 reduction by Dye/TiO_2/ReC proceeds by (1) fast electron injection from excited-singlet Dye into TiO_2, (2) transport of the injected electrons to the ReC site, and (3) the selective two-electron reduction of CO_2 to CO on ReC. An important aspect of this system is that TiO_2 can work as both an electron reservoir and an electron transporter so that ReC fixed on TiO_2 is susceptible of on-demand two-electron supply from TiO_2 followed by complex reaction processes to complete the selective reduction of CO_2 to CO on the catalyst center.[20,25] This is a major advantage of the hybrid system in achieving long-term catalytic cycles.

A further activity enhancement can be achieved with the introduction of merits of homogeneous system, which are defined as (1) an efficient antenna function without a loss of light harvesting by scattering effect and (2) fast diffusion-mediated electron transfer dynamics between components, resulting in a significant reduction of induction period in photolysis.[10,14] We call this system a binary hybrid system to discriminate it from the Dye/TiO_2/ReC "ternary" hybrid catalyst. In the binary hybrid system, excited-state PS should mediate electron transfer from an electron donor to the catalytic TiO_2/ReC particles in solution (Chart 1c). However, the organic dye (Dye) used in the ternary hybrid catalyst has a serious drawback in using it as PS in homogeneous solution, because the excited-state lifetime is too short (<1 ns) to undergo effective collisional electron transfer with either TiO_2 or ED.[26] As an alternative PS, the cationic Ir^{III}-complex is selected due to its merits such as the efficient visible-light absorption properties from single-triplet transition, a longer lifetime of excited state, and high photochemical stability.[27] Some heteroleptic Ir^{III} complexes have been successfully applied as a visible light harvester in water-splitting H_2 generation system.[27−32] However, the utilization of Ir complex as sensitizer has been still less explored in photocatalytic CO_2 reduction process.[33−35] Very recently, Ishitani et al. reported that Ir^{III} complex dyad model linked to the tricarbonyl rhenium complex has the high, durable photocatalytic CO_2 to CO conversion efficiency with its enhanced CO selectivity.[36] After having investigated some possible candidates for PS, we found that cationic iridium(III) complexes $[Ir(btp)_2(bpy\text{-}X_2)]^+$ (btp = 2-(2-pyridyl)-benzo[*b*]thiophene; X = OMe, ^{t}Bu, Me, H), which have been partially reported by Murata et al.,[37] effectively work as PS for the CO_2 reduction using the TiO_2/ReC binary hybrid catalyst. The Ir^{III} complexes have the absorption maximum at ∼430 nm with their long lifetime (3−4 μs). In this report, we discuss details of the photocatalytic CO_2-reduction behavior of the system comprising the Ir^{III}-complex-based antenna and the TiO_2/ReC binary catalyst, and the photosensitization capabilities of the Ir^{III} complexes are compared with that of $Ru(bpy)_3^{2+}$, a widely used photosensitizer, as well as with the photocatalytic behavior of the Dye/TiO_2/ReC ternary system.

EXPERIMENTAL SECTION

General Procedure. All the synthetic procedures were performed in a dry dinitrogen atmosphere. All the solvents used were distilled over sodium−benzophenone under nitrogen prior to use. Iridium(III) chloride hydrate and benzo[*b*]thien-2-ylboronic acid were purchased from Sigma-Aldrich and used without further purification. Glassware, syringes, magnetic stirring bars, and needles were dried in a convection oven for over 4 h. Reactions were monitored by thin-layer chromatography (TLC; Merck Co.). The spots developed onto TLC were identified under UV light at 254 or 365 nm. Column chromatography was performed on silica gel 60 G (particle size 5−40 μm; Merck Co.). The synthesized compounds were characterized by ^{1}H NMR, ^{13}C NMR, and high-resolution mass spectrometry (HR-MS). The ^{1}H and ^{13}C NMR spectra were recorded on a Varian Mercury 300 spectrometer (operating at 300.1 and 75.4 MHz) and Bruker Ascend 400 spectrometer in KBSI Ochang Center (operating at 400.1 and 100.6 MHz), respectively. HR-MS analysis was performed on an LC/MS/MSn (n = 10) spectrometer (Thermo Fisher Scientific, LCQ Fleet Hyperbolic Ion Trap MS/MSn Spectrometer). The absorption and emission spectra at room temperature were recorded on a UV−vis spectrophotometer (Agilent, Cary-5000) and on a fluorimeter (Varian, Cary Eclipse), respectively.

Synthesis. The Ir(III) complexes (**Ir-OMe$^+$**, **Ir-^{t}Bu$^+$**, **Ir-Me$^+$**, and **Ir-H$^+$**),[37] Re(4,4′-Y_2-2,2′-bipyridine)$(CO)_3Cl$ (**ReC** (Y = $CH_2PO_3H_2$), **RePE** (Y = $CH_2PO(OC_2H_5)_2$)),[21] organic sensitizer (dye = (*E*)-2-cyano-3-(5′-(5″-(p-(diphenylamino)phenyl)thiophen-2″-yl)thiophen-2′-yl)-acrylic acid),[38] and 1,3-dimethyl-2-phenyl-1,3-dihydrobenzimidazole (BIH)[39] were prepared by literature methods.

$[Ir(btp)_2(bpy\text{-}CN)_2]^+PF_6$ (Ir-CN$^+$). A mixture of Ir-dimer complex[40] (0.088 g, 0.068 mmol) and 4,4′-dicyano-2,2′-bipyridine[41] (bpy-CN: 0.029 g, 0.14 mmol) in ethylene glycol (5.9 mL) was heated at 150 °C for 45 h under nitrogen. The reaction mixture was poured into water (40 mL) and washed with diethyl ether (40 mL × 2). To the aqueous layer was added ammonium hexafluorophosphate (0.610 g, 3.74 mmol).

DOI: 10.1021/acs.inorgchem.7b01963
Inorg. Chem. XXXX, XXX, XXX−XXX

Chart 2. Photosensitization System in the Present Investigation on the CO_2 Reduction to CO Using the Binary Hybrid Catalyst (TiO_2/ReC), Ir-X^+ or $Ru(bpy)_3^{2+}$ as PS, and BIH as ED in DMF

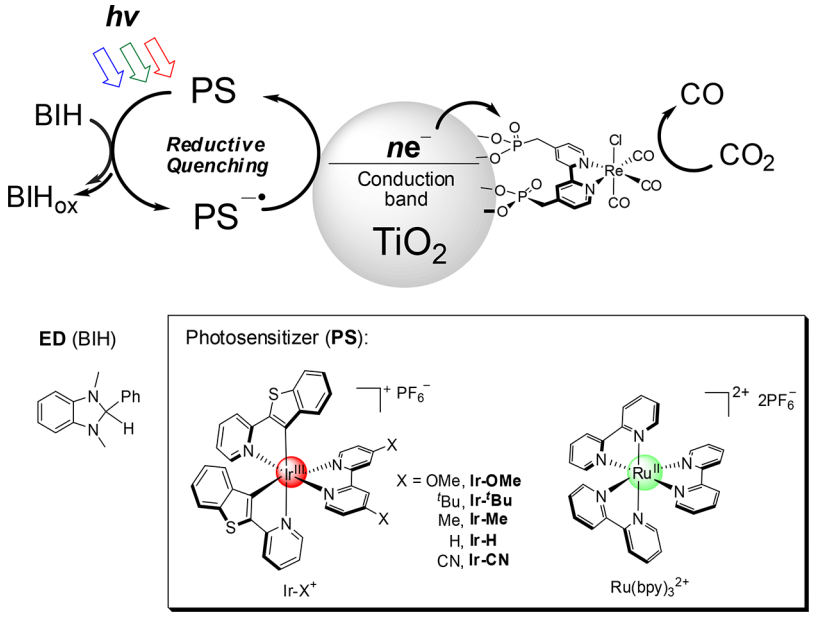

After treatment of the solution with dichloromethane (40 mL × 2), the solvent was removed by rotary evaporation under vacuum. The solids were collected by filtration, washed with water, and vacuum-dried. The obtained crude product was purified by column chromatography on silica gel (solvent: methanol/dichloromethane, 1:6 v/v), followed by recrystallization from dichloromethane through *n*-hexane vapor diffusion to yield **Ir-CN**$^+$ as dark-green crystals (0.056 g, 0.058 mmol, 85% yield). ^{1}H NMR (300 MHz, deuterated dimethyl sulfoxide (DMSO-d_6)) δ 9.54 (s, 2H), 8.13 (d, J = 7.2 Hz, 2H), 8.03−8.07 (m, 4H), 7.95 (m, 4H), 7.77 (d, J = 5.7 Hz, 2H), 7.23 (t, J = 7.5 Hz, 2H), 7.08 (t, J = 6.9 Hz, 2H), 6.88 (t, J = 8.0 Hz, 2H), 5.86 (d, J = 8.1 Hz, 2H). ^{13}C NMR (100.6 MHz, DMSO-d_6) δ 163.17, 155.69, 151.87, 150.89, 145.64, 144.61, 142.10, 140.69, 136.47, 132.10, 128.63, 125.84, 124.49, 124.15, 123.57, 122.67, 122.21, 119.99, 115.65. Electrospray ionization mass spectrometry (ESI-MS) calcd. for $C_{44}H_{36}F_6IrN_6PS_2$, 819.0977 $[M-PF_6^-]^+$; found 819 $[M-PF_6^-]^+$.

Crystal Structure Determination. Fine crystals of **Ir-H**$^+$ and **Ir-OMe**$^+$ obtained from a CH_2Cl_2/*n*-hexane solution were sealed in glass capillaries under argon and mounted on a diffractometer. The preliminary examination and data collection were performed using a Bruker SMART CCD detector system single-crystal X-ray diffractometer equipped with a sealed-tube X-ray source (50 kV × 30 mA) using graphite monochromated Mo Kα radiation (λ = 0.710 73 Å). The preliminary unit-cell constants were determined using a set of 45 narrow frame (0.3° in ω) scans. The double pass method of scanning was used to exclude noise. The collected frames were integrated using an orientation matrix determined from the narrow-frame scans. The SMART software package was used for data collection, and SAINT was used for frame integration.[42] The final cell constants were determined through global refinement of the xyz centroids of the reflections harvested from the entire data set. Structure solution and refinement were performed using the SHELXTL-PLUS software package.[42] Crystallographic data were deposited with the Cambridge Crystallographic Data Centre as supplementary publications (CCDC-1481192 (**Ir-OMe**$^+$) and CCDC-1510579 (**Ir-H**$^+$)). Additional crystallographic data are available in the Supporting Information.

Electrochemical Measurements. Cyclic voltammetry (CV) was performed on a BAS 100B electrochemical analyzer with a three-electrode cell system containing a platinum disk working electrode, a platinum wire counter electrode, and a Ag/$AgNO_3$ (0.1 M) reference. All data were obtained for an Ar-purged dimethylformamide (DMF) or CH_3CN solution containing 0.1 M tetrabutylammonium perchlorate (TBAP) at a scan rate of 50 mV s^{-1}. Absorption spectra of $[\mathbf{Ir\text{-}X}^+]^{-\bullet}$ were taken by using a spectroelectrochemical cell consisting of a Pt mesh (8 mm × 5 mm) working electrode and a Pt wire counter electrode. An Ar-purged CH_3CN solution containing **Ir-X**$^+$ (1 mM) and TBAP (0.1 M) was electrolyzed at −1.6 V with a BAS 100B electrochemical analyzer using an Ag/$AgNO_3$ reference electrode.

Time-Resolved Emission-Lifetime Measurement. Phosphorescence lifetime measurements of **Ir-X**$^+$ in CH_3CN in the absence of TiO_2 were made with an ICCD (Andor, iStar) attached on a monochromator (DongWoo Optron, Monora500i). The excitation light was the 416 nm beam generated through the H_2 Raman shifter seeded with the third harmonic output (355 nm) of a Q-switched Nd:YAG laser (Continuum, Surelite II). Comparable measurements of the phosphorescence decays in the presence and absence of TiO_2 dispersions were undertaken with a picosecond fluorescence lifetime measurement system using a Hamamatsu streak camera (C11200). An ultrashort laser pulse was generated with a Ti:sapphire oscillator (Spectra Physics, MaiTai SP) pumped with a diode solid-state laser, and high power pulses at 430 nm were generated using a Ti:sapphire regenerative amplifier (Spectra Physics, Spitfire Ace) and an optical parametric amplifier (Spectra Physics, TOPAS prime).

Measurement for Decay of Photogenerated PS$^{-\bullet}$. The decay profiles of PS$^{-\bullet}$ (Figure 8 and S6) were monitored at 529 ± 15 nm (λ_{max} of $[\mathbf{Ir\text{-}X}^+]^{-\bullet}$ or $[Ru(bpy)_3^{2+}]^{-\bullet}$) with a bandwidth of 4 nm on an Agilent Cary-5000 spectrometer operated at an averaged sampling time of 33 ms, after PS$^{-\bullet}$ had been generated by 2 min of irradiation of an Ar-purged 3 mL DMF/H_2O mixture solvent (2.5 vol % H_2O) containing 25 μM PS (**Ir-X**$^+$ or $Ru(bpy)_3^{2+}$) and 2.5 mM BIH in the absence or presence of 5 mg of TiO_2 or a 12 μm thick mesoporous TiO_2 film (7 mm × 20 mm); it was confirmed by preliminary experiments that the irradiation time of 2−5 min is sufficient for the complete conversion of PS to PS$^{-\bullet}$ (see Figures 9 and S7). In the experiment on the enhanced bleaching of the 529 nm absorption in the presence of 5 mg of TiO_2 particles (Figure 8), both irradiation and monitoring were undertaken without agitation of the sample after complete precipitation of visible TiO_2 particles dispersed in solution by Ar bubbling.

Preparation of TiO_2/ReC Catalyst. Commercially available TiO_2 particles (Hombikat UV-100, Huntsman) with specific Brauner−Emmet−Teller (BET) surface areas of greater than 250 m^2/g were thoroughly washed with distilled water, ultrasonically treated in water, separated by centrifugation, and then dried in an oven under N_2. The TiO_2 particles (100 mg) were stirred overnight in a 50 mL solution of ReC (*fac*-[Re(4,4′-bis(dihydroxyphosphorylmethyl)-2,2′-bipyridine)$(CO)_3Cl$]) (1 μmol) in CH_3CN/*tert*-butanol, and then subjected to centrifugation.

DOI: 10.1021/acs.inorgchem.7b01963
Inorg. Chem. XXXX, XXX, XXX−XXX

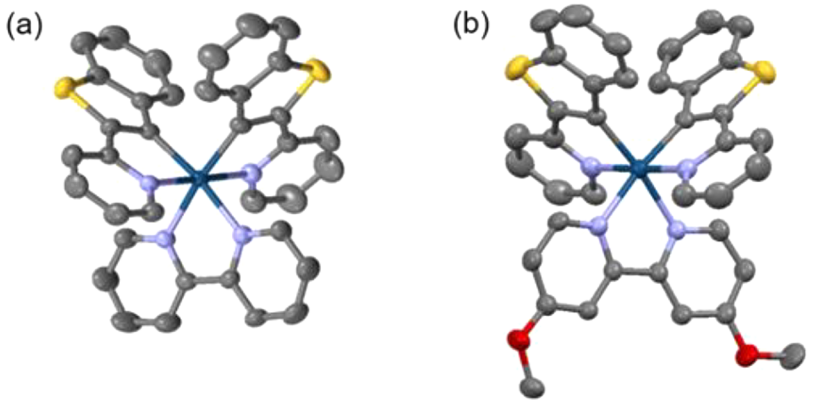

Figure 1. Structure of (a) **Ir-H**$^+$ and (b) **Ir-OMe**$^+$ obtained by X-ray crystallographic analysis. Displacement ellipsoids are drawn at the 30% probability level, and H atoms were omitted for clarity.

Table 1. Photophysical Properties of Ir-X$^+$

	λ_{abs}[a] (nm) (ε (1×10^3 M^{-1} cm^{-1}))	λ_{em}[b] (nm)	Φ_{PL}[c]	τ[d] (μs)	k_r[e] (1×10^4 s^{-1})	k_{nr}[f] (1×10^5 s^{-1})
Ir-OMe$^+$	268(38), 328(21), 427(6)	591, 640, 701	0.107	5.64	1.90	1.58
Ir-^{t}Bu$^+$	272(34), 309(26), 327(19), 430(6)	589, 638, 702	0.116	6.47	1.79	1.37
Ir-Me$^+$	272(31), 308(24), 326(18), 427(6)	590, 638, 703	0.064	4.39	1.46	2.13
Ir-H$^+$	277(33), 311(25), 335(18), 431(6)	590, 641 712	0.009	0.255	3.53	38.9
Ir-CN$^+$	284(39), 310(31), 327(26), 401(8), 429(7), 560(0.3)	[g]	[g]	[g]	[g]	[g]
$Ru(bpy)_3^{2+}$ [h]	244(25), 287(84), 451(14)	621	0.095	0.855	10.6	10.2

[a]Absorption maxima (molar extinction coefficient). [b]Phosphorescence maxima. [c]Phosphorescence quantum yield measured in deaerated acetonitrile. [d]Phosphorescence lifetime measured in deaerated acetonitrile. [e]Radiative rate constant. [f]Nonradiative rate constant. [g]No luminescence. [h]Reference10. All experiments are measured at room temperature.

The collected solids were washed with the solvent and then dried in an oven under N_2. The successful anchoring of ReC on TiO_2 was confirmed by the IR absorption bands characteristic of the CO ligands at 2025, 1920, and 1910 cm^{-1}. The complete loading of ReC was confirmed by absorbance comparison before and after adsorption step of ReC: the supernatant, which is separated after centrifugation of the ReC treated suspensions, showed the negligible absorption intensity of ReC (Figure S9).

Photocatalyzed CO_2 Reduction. Suspensions of TiO_2/ReC particles (0.1 μmol ReC on 10 mg TiO_2) in 3 mL of DMF containing 1 mM PS (**Ir-X**$^+$ or $Ru(bpy)_3^{2+}$), 0.1 M BIH, and 2.5 vol % H_2O were placed in a pyrex cell (~1 cm pass length; 6.0 mL total volume), bubbled with CO_2 for 30 min, sealed with a septum, and then irradiated under stirring with visible light at greater than 400 nm emitted from a light-emitting diode (LED) lamp (60 W, Cree Inc.). Homogeneous-solution photoreactions were performed in 3 mL of DMF solutions containing **Ir-X**$^+$ (0.5 mM), RePE (0.5 mM), and BIH (0.1 M). The amounts of CO evolved in the overhead space of the cell were determined by gas chromatography (HP6890A GC equipped with a TCD detector) using a 5 Å molecular sieve column. The liquid phase of the irradiated samples was subjected to HPLC analysis using a Waters 515 pump, a Waters 486 UV detector operated at 210 nm, a Rspak KC-811 Column (Shodex), and 0.05 M H_3PO_4 aqueous solution eluent.

RESULTS AND DISCUSSION

Synthesis. Chart 2 illustrates a schematic representation of the present photosensitization system and the structures of the molecules used in this work. The cationic Ir^{III}-complexes denoted as **Ir-X**$^+PF_6^-$ (X = OMe, ^{t}Bu, Me, H, and CN) were synthesized from dimeric $Ir_2(btp)_4Cl_2$ and 4,4′-X_2-2,2′-bipyridines (X_2-bpy) in moderate yields.[37] The preparation of $Ru(bpy)_3^{2+}(PF_6^-)_2$ used as a comparative photosensitizer was performed according to the published method.[43] The structures of **Ir-X**$^+PF_6^-$ were confirmed by spectroscopic and elemental analyses. In particular, **Ir-H**$^+PF_6^-$ and **Ir-OMe**$^+PF_6^-$ gave fine crystals suitable for X-ray crystallographic analysis, revealing monoclinic $P2_1/n$ and $P2_1/c$ space group with reliability factors of R_1 = 0.0315 and 0.0286, respectively. Details of the crystal structures are summarized in Tables S1−S5. As shown in Figure 1 for ORTEP drawings, the (2-pyridyl)benzo[*b*]thiophen-3-yl ligands are commonly bonded to the iridium(III) center with *cis*-C,C and *trans*-*N*,*N* dispositions.[44]

Photophysical and Electrochemical Properties of Ir-X$^+$. The UV−visible absorption and emission spectra of **Ir-X**$^+$ were measured in acetonitrile. The absorption maxima and molar extinction coefficients are listed in Table 1. As shown in Figure 2, all complexes commonly reveal intense absorptions at ~250 and ~350 nm assignable as the $\pi-\pi^*$ transitions of the X_2-bpy and btp ligands, respectively, and a less intense absorption band at ~430 nm attributable to a transition with a dominant contribution of Ir^{III}-to-btp charge transfer.[37] In the case of **Ir-CN**$^+$, an extra weak band appears around 560 nm, which is attributable to an insignificant contribution of metal-ligand-to-ligand charge transfer (^{1}MLLCT) transition related to the bipyridine ligand and lowest unoccupied molecular orbital (LUMO) level lowered by two electron-withdrawing CN substituents as reported for another **Ir-X**$^+$ complex (X = CF_3).[37]

The emission spectra of **Ir-X**$^+$ taken in degassed acetonitrile at room temperature are shown in Figure 2b, and the data are listed in Table 1. The phosphorescence diagram and data at 77 K are shown and summarized in Figure S10 and Table S7, respectively (see Supporting Information). The Ir(III) complexes reveal similar phosphorescence spectra with the maxima at ~590 and ~640 nm accompanied by a shoulder at ~701 nm, while **Ir-CN**$^+$ is virtually nonemissive even at 77 K. As shown in Table 1, the quantum yields (Φ) and lifetimes (τ) of phosphorescence for the four emissive complexes uniquely depend on the substituent (X) of the bpy ligand. From the observed values of Φ and τ, the rate

DOI: 10.1021/acs.inorgchem.7b01963
Inorg. Chem. XXXX, XXX, XXX−XXX

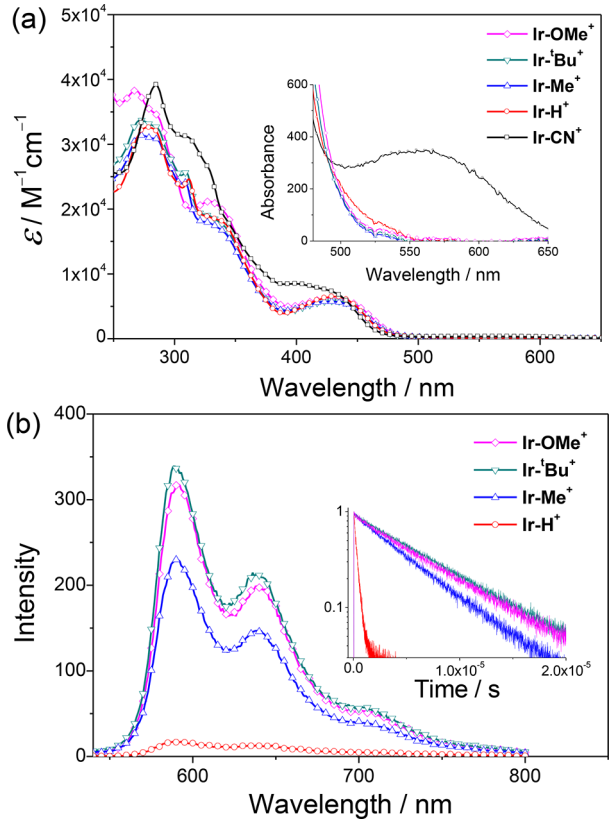

Figure 2. Absorption spectra of **Ir-X**$^+$ in acetonitrile (a). (inset) Expanded view for the low-energy spectral region. Emission spectra of **Ir-X**$^+$ (10 μM) taken by excitation at 300 nm in acetonitrile at room temperature (b). (inset) Phosphorescence decay profiles of **Ir-X**$^+$ in acetonitrile at room temperature.

constants of the radiative (k_r) and nonradiative pathways (k_{nr}) were calculated. While the k_r values are similar for the emissive complexes with minor differences, k_{nr} increases in the order **Ir-OMe**$^+$ ≈ **Ir-**^{t}**Bu**$^+$ < **Ir-Me**$^+$ ≪ **Ir-H**$^+$, an interesting dependence on the bulkiness and/or electron-donating character of X. Since the emissive complexes reveal almost identical phosphorescence spectra and similar k_r values independently of the X_2-bpy ligand, the btp ligand should be dominantly involved in the emissive excited state accompanied by a small or negligible contribution of the X_2-bpy ligand. On the one hand, the phosphorescence of **Ir-X**$^+$ should commonly occur from a state with a dominant or major contribution of the btp-centered triplet (^{3}LC) mixed with a metal-to-ligand charge-transfer (^{3}MLCT) character, as reported for similar heteroleptic[37,44] and homoleptic[45,46] Ir^{III} analogues with the btp ligand. On the other hand, the k_{nr} values significantly vary with X, suggesting that the X_2-bpy ligands significantly contribute to the nonradiative decay process (or processes) from the emissive state.

A possible assumption is that vibrational modes in the X_2-bpy ligands would be more or less coupled with the crossing from the emissive state to other nonemissive state(s), for example, a metal-centered triplet state (^{3}MC).[47] Alternatively, the electron-donating OMe, ^{t}Bu, and Me substituents would more or less enhance the electron density on the Ir(III) center in the excited state to result in an increase of the barrier for the crossing to the nonradiative state(s). In the case of **Ir-CN**$^+$, the strong electron-withdrawing effect of the two CN substituents should cause a significant reduction of the electron density on the metal center to result in a barrierless crossing to the putative ^{3}MC state. Alternatively, the lowest-excited singlet state of **Ir-CN**$^+$ different from that of the other complexes would undergo direct inter-system crossing to a nonemissive triplet state. At any rate, if the nonemissive state would be coupled with a chemical change of **Ir-X**$^+$, the Ir(III) complexes are not attractive as PS. Fortunately, it was confirmed that all the complexes are totally stable under long-term irradiation in DMF (Figure S11), an observation suggesting that **Ir-X**$^+$ can work as potential photosensitizer for the present CO_2-reduction investigation.

The electrochemical properties of **Ir-X**$^+$ were examined by cyclic voltammetry (CV), the data of which are summarized in Table 2. Typical CV scans of **Ir-X**$^+$ are shown in Figure 3,

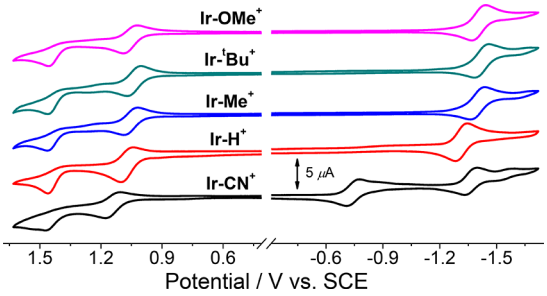

Figure 3. CVs of **Ir-X**$^+$ (1 mM) in the oxidation (left) and reduction (right) sides in CH_3CN in the presence of 0.1 M TBAP; scan rate at 50 mV s^{-1}.

revealing quasi-reversible behavior with distinct anodic and cathodic waves in both the positive (oxidation) and negative (reduction) sides, from which the half-wave oxidation and reduction potentials, $E_{1/2}^{ox}$ and $E_{1/2}^{red}$, were estimated. The $E_{1/2}^{ox}$ values are almost identical within 30 mV differences except for **Ir-CN**$^+$ where the potential is more positive by 70−100 mV.

Since the highest-occupied molecular orbital (HOMO) can be considered to dominantly populate on the Ir(III) center,[49] the

Table 2. Electrochemical Data and Related Energy Levels for PSs

	$E_{1/2}^{ox}$ [a] [V]	$E_{1/2}^{red}$ [a] [V]	E_{0-0} [b] [eV]	HOMO[c] [eV]	LUMO[c] [eV]	E_{red}* [d] [V]	E_{ox}* [e] [V]
Ir-OMe$^+$	1.06	−1.41	2.13	−5.48	−3.01	0.72	−1.07
Ir-^{t}**Bu**$^+$	1.04	−1.42	2.13	−5.46	−3.00	0.71	−1.09
Ir-Me$^+$	1.05	−1.40	2.13	−5.47	−3.02	0.73	−1.08
Ir-H$^+$	1.07	−1.31	2.13	−5.49	−3.11	0.82	−1.06
Ir-CN$^+$	1.14	−0.74	2.12	−5.56	−3.68	1.19	−0.79
$Ru(bpy)_3^{2+}$	1.25	−1.34	2.14[f]	−5.67	−3.08	0.80	−0.89

[a] E_{pa} = anodic peak potential, E_{pc} = cathodic peak potential, and $E_{1/2} = (E_{pc} + E_{pa})/2$ versus SCE. [b] E_{0-0} denotes triplet energy estimated from the phosphorescence data at 77 K. [c] HOMO and LUMO levels were determined using the following equations: E_{HOMO} (eV) = $-e(E_{1/2}^{ox} + 4.42)$; E_{LUMO} (eV) = $-e(E_{1/2}^{red} + 4.42)$. [d] Excited-state reduction potential estimated using $E_{red}^* = E_{1/2}^{red} + E_{0-0}$. [e] Excited-state oxidation potential estimated using $E_{ox}^* = E_{1/2}^{ox} - E_{0-0}$. [f] Reference 48.

DOI: 10.1021/acs.inorgchem.7b01963
Inorg. Chem. XXXX, XXX, XXX−XXX

energy levels would be not significantly changed by the OMe and alkyl substituents of X_2-bpy. In the case of X = CN, however, the strong electron-withdrawing effect of CN would cause an appreciable decrease of electron density on the metal center to result in a slight positive shift of the HOMO level. On the one hand, with respect to the reduction potential, the $E_{1/2}^{red}$ values in the cases of X = OMe, ^{t}Bu, and Me are again similar within 20 mV differences but more negative by ~100 mV than that of **Ir-H$^+$**. On the other hand, **Ir-CN$^+$** reveals a substantially more positive shift of $E_{1/2}^{red}$ by 570−680 mV. These results show that the LUMO level of **Ir-X$^+$** is more sensitive to the electron-donating and electron-withdrawing character of the substituent X on the bpy ligand than the HOMO level.

Photocatalytic CO_2 Reduction. The hybrid catalyst (TiO_2/ReC) was prepared by anchoring of Re(4,4′-Y_2-bpy)$(CO)_3$Cl (ReC = ReP; Y = $CH_2PO_3H_2$) on TiO_2 particles as described in our previous papers.[20,21] Suspensions of TiO_2/ReC particles in CO_2-saturated DMF containing PS (**Ir-X$^+$** or $Ru(bpy)_3^{2+}$, 1 mM), BIH (0.1 M), and 2.5 vol % H_2O were irradiated at greater than 400 nm using an LED lamp (60 W, Cree Inc.). With **Ir-X$^+$** (X = H, Me, ^{t}Bu, and OMe) as PS, the photoreactions gave CO as the major CO_2-reduction product accompanied by small amounts of HCOOH and H_2. In the absence of either PS or BIH, formation of CO was much less efficient or not detected at all (Table S8). Figure 4 shows plots of TN_{CO} (= molar ratio of CO

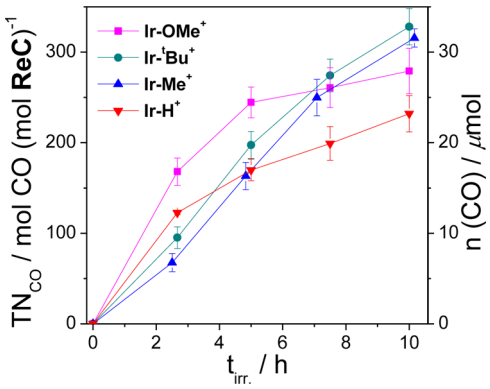

Figure 4. Comparable plots of TN_{CO} versus irradiation time for the four **Ir-X$^+$** sensitizers; irradiation at greater than 400 nm for dispersions of 10 mg TiO_2/ReC (0.1 μmol) in CO_2-saturated DMF involving 1 mM **Ir-X$^+$** and 0.1 M BIH and 2.5 vol % H_2O. The vertical error bar at each data point is based on experimental data repeated four times.

formed/ReC used) versus irradiation time. After 4 h of irradiation, TN_{CO} reaches ~180 with **Ir-OMe$^+$** and 120−140 with the others except for **Ir-CN$^+$**; **Ir-CN$^+$** is inactive as PS. On the one hand, it is of significance to note that **Ir-OMe$^+$** reveals the highest photosensitization efficiency at an initial stage of the reaction but shows leveling-off behavior after 2 h of irradiation (Figure 4), probably due to net chemical changes of **Ir-OMe$^+$** during the photosensitization. On the other hand, the TN_{CO} plots for **Ir-^{t}Bu$^+$** and **Ir-Me$^+$** are linear up to 10 h to give ~300 of TN_{CO}, demonstrating that both **Ir-^{t}Bu$^+$** and **Ir-Me$^+$** are less efficient but much more stable as PS than **Ir-OMe$^+$**.

For comparison, the other photosensitization systems (Chart 1a,b) were applied to the photocatalytic reduction of CO_2 under similar conditions, that is, (1) a binary hybrid system using $Ru(bpy)_3^{2+}$ as PS in place of **Ir-X$^+$** (abbreviated as $Ru(bpy)_3^{2+}$−TiO_2/ReC), (2) a homogeneous system using **Ir-OMe$^+$** as PS and RePE as CO_2 reduction catalyst (**Ir-OMe$^+$**−RePE), and (3) the Dye/TiO_2/ReC ternary hybrid system. Figure 5 and

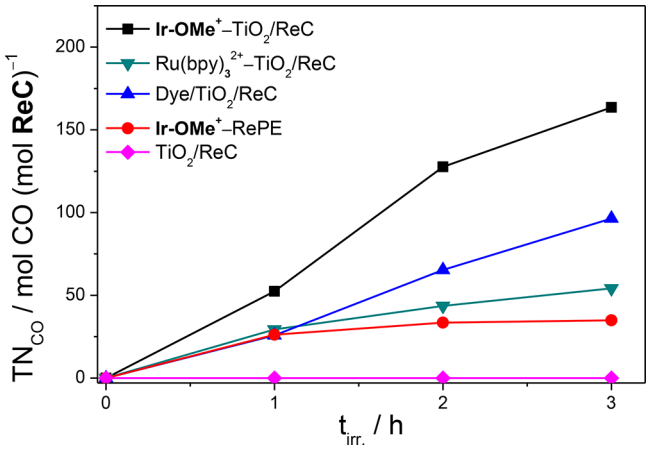

Figure 5. Plots of TN_{CO} vs irradiation time for the binary systems of **Ir-OMe$^+$**−TiO_2/ReC (black ■) and $Ru(bpy)^{2+}$−TiO_2/ReC (inverted ▼), the Dye/TiO_2/ReC ternary system (blue ▲), the **Ir-OMe$^+$**−RePE homogeneous system (red ●), and the TiO_2/ReC catalyst in the absence of PS (pink ◆).

Table 3 show CO formation (TN_{CO} and μmol) versus irradiation time for these systems compared with that for the binary hybrid

Table 3. Comparison of Four Different Reaction Systems in Visible Light Driven CO Production

			amount of CO produced @3 h
system	PS/ μmol	ReC/ μmol	TON
Ir-OMe$^+$−TiO_2/ReC	3	0.1	163
Ru(bpy)$_3^{2+}$−TiO_2/ReC	3	0.1	54
Dye/TiO_2/ReC	1.5	0.1	96
Ir-OMe$^+$−RePE	1.5	1.5	35

system using **Ir-OMe$^+$** as PS (**Ir-OMe$^+$**−TiO_2/ReC). In the case of $Ru(bpy)_3^{2+}$−TiO_2/ReC, leveling-off behavior of TN_{CO} appears even at an early stage to give a low TN_{CO} (~50) after 3 h of irradiation, considerably lower than those of **Ir-X$^+$**−TiO_2/ReC, demonstrating that **Ir-X$^+$** works as a much more efficient and persistent photosensitizer than $Ru(bpy)_3^{2+}$. For the **Ir-OMe$^+$**−RePE homogeneous system, the CO formation is leveled off even at 1 h of irradiation to give a very low TN_{CO} (~30; Figure S12). As previously stated,[17,20−23,25] the hybridization of ReC with TiO_2 enables the catalyst to persistently work, providing a potential strategy for designing efficient catalytic systems based on molecular catalysts. It is of interest to note that TN_{CO} of the Dye/TiO_2/ReC ternary system is ~1.8-fold lower than that of the **Ir-OMe$^+$**−TiO_2/ReC binary system and significantly lower than those of the binary system using the other **Ir-X$^+$** sensitizers (X = ^{t}Bu, Me, and H), perhaps due to light-scattering effects in the ternary system. The apparent quantum yield (AQY) of CO production at 436 nm for the binary hybrid system (**Ir-OMe$^+$**−TiO_2/ReC) in the presence of 2.5 vol % water was determined to be $(3.7 \pm 0.2) \times 10^{-2}$, which is ~2 times higher than the ternary system (Table S8). An ^{13}C isotope tracer experiment was performed for the binary hybrid system (**Ir-^{t}Bu$^+$**−TiO_2/ReC) in $^{13}CO_2$−saturated DMF-d_7−D_2O mixed solvent (2.5 vol % D_2O) containing 0.1 M BIH. A sharp signal at 184.5 ppm and the ^{13}C isotope abundance (>98.7%) of the produced CO gas analyzed by ^{13}C NMR spectrum (DMF-d_7) and gas chromatography−mass spectrometry (GC-MS), respectively, indicate that the CO originated from injected CO_2 gas (Figures S13 and S14).

DOI: 10.1021/acs.inorgchem.7b01963
Inorg. Chem. XXXX, XXX, XXX−XXX

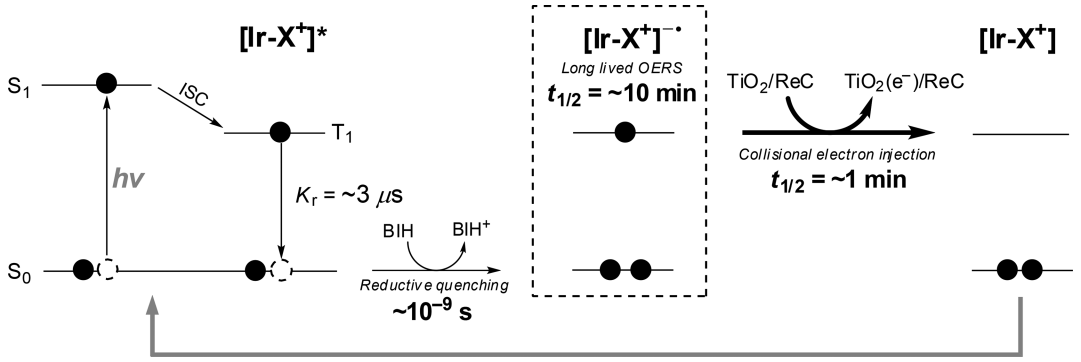

Figure 6. Schematic representation showing photoexcitation to a singlet excited (S_1), intersystem crossing (ISC) to a triplet excited state (T_1), long-lived OERS of [**Ir-X**$^+$] ([**Ir-X**$^+$]$^{-\bullet}$) formed with fast reductive quenching process, and a slow collisional electron injection from [**Ir-X**$^+$]$^{-\bullet}$ to TiO_2/ReC. Note that energy levels in this diagram are not determined based on an experimental evidence and do not reveal the exact values.

DISCUSSION

$$^3PS^* + BIH \rightarrow PS^{-\bullet} + BIH^+ \quad (PS = \textbf{Ir-X}^+ \text{ or } Ru(bpy)_3^{2+}) \tag{1}$$

$$PS^{-\bullet} + TiO_2/ReC \rightleftarrows PS - - - TiO_2(e^-)/ReC \rightarrow PS + TiO_2/ReC^{-\bullet} \tag{2}$$

$$TiO_2/ReC^{-\bullet}(L(CO)_3ReCl^{-\bullet}) \rightarrow TiO_2/L(CO)_3Re^{\bullet} + Cl^- \tag{3}$$

$$TiO_2/L(CO)_3Re^{\bullet} + DMF \rightleftarrows TiO_2/L(CO)_3Re^{\bullet}(DMF) \tag{4}$$

$$TiO_2(e^-)/L(CO)_3Re^{\bullet}(DMF) + CO_2 \rightleftarrows TiO_2/L(CO)_3Re^{\bullet}(CO_2) + DMF \tag{5}$$

$$TiO_2(e^-)/L(CO)_3Re^{\bullet}(CO_2) + 2H^+ \rightarrow \rightarrow TiO_2/ReC + CO + H_2O \tag{6}$$

Equations 1−6 show essential reaction processes for discussing structure−reactivity relationships in the present photosensitized CO_2 reduction based on the binary system. The initiation process for the photosensitized CO_2 reduction in either the binary hybrid system or the homogeneous system should be electron transfer from BIH to triplet-state PS (^{3}PS* = ^{3}**Ir-X**$^+$* or $^3Ru(bpy)_3^{2+}$*) to generate the one-electron reduced species (OERS) of PS (PS$^{-\bullet}$; eq 1). This is supported by the complete phosphorescence quenching by 0.1 M BIH for each of PS. Figure S15 shows a Stern−Volmer plot for quenching of the **Ir-**^{t}**Bu**$^+$ phosphorescence by BIH as a typical example; the quenching rate constant was calculated from the slope of the plot and the phosphorescence lifetime to be 5.9×10^8 M^{-1} s^{-1}. This is in accord with the sufficiently negative free-energy changes of eq 1 (ΔG_1 = −(0.46−0.94) eV) calculated from the excited-state reduction potentials of ^{3}PS* (E_{red}* = 0.72−1.19 V vs standard calomel electrode (SCE) for **Ir-X**$^+$ and 0.80 V for $Ru(bpy)_3^{2+}$) and the oxidation potential of BIH ($E_{1/2}^{ox}$ = 0.25 V).[22] Furthermore, irradiation of a DMF solution containing **Ir-X**$^+$ and BIH for 5 min gave a new absorption spectrum with the maximum at 510−540 nm, which is essentially identical with the spectrum of [**Ir-X**$^+$]$^{-\bullet}$ taken by spectroelectrochemical measurements of **Ir-X**$^+$ (Figures S7 and S16). Note that there might be two different reduction pathways for the ^{3}PS* by BIH; one is related to the electron transfer suggested by this work and the other to the hydride transfer suggested by the recent report[50] of Bao and co-workers. However, we think the reductive quenching in our hybrid system is preferably taking place following electron transfer mechanism rather than hydride transfer, since previous reports by Ishitani and co-workers,[51−53] which resemble our PSs closely, presented the detailed experimental evidence supporting the reductive quenching of PS* (Ru^{II} or Ir^{II}) by electron transfer mechanism (Figure 6). An alternative initiation process would be the direct electron injection from ^{3}PS* into TiO_2. However, this process is unlikely to occur, because decay profiles of the **Ir-**^{t}**Bu**$^+$ phosphorescence are unchanged in the presence of dispersed TiO_2 particles (Figure S17). In accord with this, the excited-state oxidation potential of ^{3}PS* (E_{ox}* = −(0.79−1.09 V)) is considerably less negative than the flat-band potential (E_{fb} = −1.50 V) of a TiO_2 nanoparticle film in DMF in the presence of 3% water.[18] For the homogeneous photosensitization, electron transfer from ^{3}**Ir-X**$^+$* to RePE would be another possible process apart from eq 1. However, quenching of the **Ir-**^{t}**Bu**$^+$ phosphorescence by RePE was very inefficient; a Stern−Volmer plot gave a rate constant of ~1×10^6 M^{-1} s^{-1} (Figure S18 and Table S10), which is smaller by 2 orders of magnitude than that for quenching by BIH.

The second important process is collisional electron injection from PS$^{-\bullet}$ into TiO_2 followed by transport of the injected electron ($TiO_2(e^-)$) to ReC (eq 2). On the one hand, the electron injection should depend on the differences between the conduction-band edge of TiO_2 and the reduction potentials ($E_{1/2}^{red}$) of PS. On the other hand, the conduction-band edge of TiO_2 is known to be close to the experimentally determined flat-band potential (E_{fb}), which is ca. −1.50 V versus SCE for a TiO_2 *nanoparticle film* in the presence of 3 vol % water in DMF.[20] If the E_{fb} value is applicable to the present TiO_2 *particles dispersed* in DMF, the electron injection from PS$^{-\bullet}$ into TiO_2 should be endergonic by 0.08−0.19 eV (Figure 7).

Under such conditions, the electron injection might be slow, probably proceeding in equilibrium with electron reversal from $TiO_2(e^-)$ to PS. It should be, however, noted that each PS$^{-\bullet}$ generated by irradiation of PS in the presence of BIH in DMF can survive with half lifetimes ($t_{1/2}$) of 10−19 min for [**Ir-X**$^+$]$^{-\bullet}$ and 5.5 min for $[Ru(bpy)_3^{2+}]^{-\bullet}$ in the absence of TiO_2 (Figure S6 in Supporting Information), long-lived enough for effective electron injection into TiO_2 to occur. Such a long lifetime of OERS is very unusual, although Fukuzumi and co-workers[54−56] reported previously a photoinduced long-lived charge separation (~a few hundred milliseconds to seconds) in a series of dopant−host dyad systems created from either covalent bond or electrostatic

DOI: 10.1021/acs.inorgchem.7b01963
Inorg. Chem. XXXX, XXX, XXX−XXX

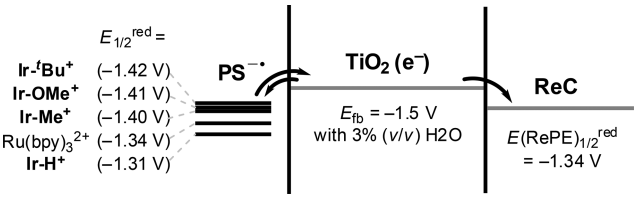

Figure 7. Relative energy levels (V vs SCE) of the flat-band potential (E_{fb}) of TiO_2, the reduction potentials ($E_{1/2}^{red}$) of PS, and the reduction potential of ReC (represented by that of RePE ($E(RePE)_{1/2}^{red}$)).

interaction. However, it is probable that the OERS of PS can survive for a long period of time when there are no quenching pathways available in the presence of strong two-electron reductant, BIH. This was confirmed by the observation that the decay of $[\mathbf{Ir}\text{-}^t\mathbf{Bu}^+]^{-\bullet}$ is considerably accelerated in the presence of TiO_2, as shown in Figure 8. The similar decay acceleration in the

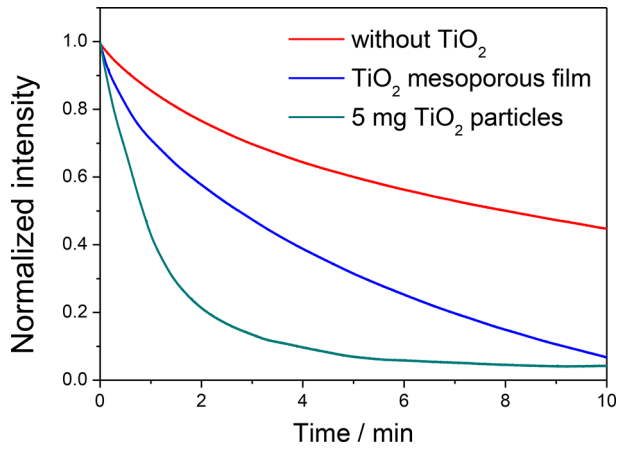

Figure 8. Normalized decay profiles of the absorption at 529 nm (λ_{max} of $[\mathbf{Ir}\text{-}^t\mathbf{Bu}^+]^{-\bullet}$) in the dark after 2 min of irradiation of 3 mL of DMF solution of 25 μM $\mathbf{Ir}\text{-}^t\mathbf{Bu}^+$, 2.5 mM BIH, and 2.5 vol % H_2O in the absence of TiO_2 (red line), with 5 mg of TiO_2 particles placed in the bottom of the cell (green line), and with a mesoporous TiO_2 film dipped in the solution (blue line).

presence of TiO_2 particles is also apparent for the other $\mathbf{Ir}\text{-}\mathbf{X}^+$ sensitizers (X = OMe, Me, and H; Figures S19 and S20). After DMF solutions of $\mathbf{Ir}\text{-}^t\mathbf{Bu}^+$ and BIH in the absence and presence of 5 mg of TiO_2 particles placed in the bottom of the cell had been irradiated for 5 min, the absorption at 529 nm (λ_{max} of $[\mathbf{Ir}\text{-}^t\mathbf{Bu}^+]^{-\bullet}$) grown by the irradiation was monitored in the dark. During the irradiation and monitoring, the solutions were kept under stationary conditions to minimize dispersing of the TiO_2 particles. Otherwise, dispersed TiO_2 particles should extensively scatter the incident light to disturb reliable optical measurements. Even under such conditions, the decay of the $[\mathbf{Ir}\text{-}^t\mathbf{Bu}^+]^{-\bullet}$ absorption was considerably faster in the presence of TiO_2 than in its absence. Probably, the accelerated bleaching of the 529 nm absorption should occur as the consequence of electron injection from $[\mathbf{Ir}\text{-}^t\mathbf{Bu}^+]^{-\bullet}$ into a small amount of colloidal TiO_2 nanoparticles (e.g., 4−5 nm size primary particles) floating in solution and, perhaps, into the TiO_2 agglomerate particles situated in the bottom of the cell. Another experiment using a TiO_2 mesoporous film immersed in solution of $[\mathbf{Ir}\text{-}^t\mathbf{Bu}^+]$ and BIH revealed again enhanced bleaching of the 529 nm absorption. While the decay profile in Figure 8 is not relevant to kinetic analysis, the electron injection from $[\mathbf{Ir}\text{-}^t\mathbf{Bu}^+]^{-\bullet}$ into TiO_2 should be complete under the CO_2-reduction conditions, where 10 mg of TiO_2/ReC particles are fully dispersed in solution by stirring. In fact, the absorption of $[\mathbf{Ir}\text{-}^t\mathbf{Bu}^+]^{-\bullet}$ was not observed at all after 1 h of irradiation of TiO_2-dispersed solution containing $\mathbf{Ir}\text{-}^t\mathbf{Bu}^+$ and BIH (Figure S21).

Under such circumstances where the electron injection process (eq 2) is slightly endergonic, it can be presumed that the net efficiency of electron transport to ReC would be sensitively affected by various factors such as the small differences in $E_{1/2}^{red}$, steric properties of PS, and distributions of the odd electron in $PS^{-\bullet}$. Provided the photosensitization efficiencies in the early stage of the reaction are related to the amounts of injected electrons, it is of interest to note that $\mathbf{Ir}\text{-}\mathbf{OMe}^+$ is significantly more efficient as photosensitizer than $\mathbf{Ir}\text{-}^t\mathbf{Bu}^+$ and $\mathbf{Ir}\text{-}\mathbf{Me}^+$ even though the $E_{1/2}^{red}$ differences are only 10−20 mV. Presumably, the strong electron-donating effect of the two OMe substituents would prevent significant population of the odd electron on the bpy ligand to push the odd electron toward the btp ligand. The particular electronic character of $[\mathbf{Ir}\text{-}\mathbf{OMe}^+]^{-\bullet}$ might be indicated by the broad spectrum different from the common sharp spectra for other $[\mathbf{Ir}\text{-}\mathbf{X}^+]^{-\bullet}$ (Figures S7d and S16d).

The reduction of CO_2 to CO requires net two-electron transfer to ReC from $TiO_2(e^-)$, which should sequentially proceed. The simultaneous transfer of two electrons as an alternative process is unlikely to occur, because E_{fb} of TiO_2 is considerably less negative than the two-electron reduction potential of ReC (−1.72 V vs SCE).[57] The one-electron reduced species of ReC ($ReC^{-\bullet} = L(CO)_3ReCl^{-\bullet}$) generated by the initial one-electron transfer from $TiO_2(e^-)$ to ReC gives the 17-electron species ($L(CO)_3Re^{\bullet}$) as a key intermediate after the liberation of Cl^- (eq 3) followed by coordination of a solvent molecule (eq 4).[58−63] This species is known to interact with CO_2,[64,65] probably by the coordination of CO_2 to the metal center (eq 5). Although the follow-up processes have not been fully explored, the second electron transfer should occur with electrons deposited in TiO_2 after the coordination of CO_2 to complete the CO_2 reduction under participation of protons (eq 6). These chemical processes (eqs 3−6) might be slower than the electron-transfer processes (eqs 1 and 2)[17,66] to result in a situation with a mismatch between the electron flow and the chemical processes. As the consequence, $PS^{-\bullet}$ might be increasingly accumulated in solution with elapsing of irradiation time after TiO_2 has been filled with electrons. In cases where $PS^{-\bullet}$ would undergo chemical changes during the CO_2-reduction catalytic cycles, the efficiency of photosensitized CO formation should start to drop after PS has been significantly consumed. This might lead to the leveling-off behavior of photosensitized CO formation observed in a later stage of the reaction. The lower the chemical stability of $PS^{-\bullet}$, the sooner the leveling-off behavior would appear.

Figure 9 shows changes of absorption spectra following irradiation time for Ar-purged DMF solution containing $\mathbf{Ir}\text{-}\mathbf{X}^+$ (X = OMe or ^{t}Bu) and BIH in the absence of TiO_2. Upon irradiation of the solution for 5 min, the spectrum of $\mathbf{Ir}\text{-}\mathbf{X}^+$ was completely changed to a new one with the longest absorption maximum at ~529 nm, which is the same as that of $[\mathbf{Ir}\text{-}\mathbf{X}^+]^{-\bullet}$ observed by spectroelectrochemistry. This indicates the complete conversion of $\mathbf{Ir}\text{-}\mathbf{X}^+$ to $[\mathbf{Ir}\text{-}\mathbf{X}^+]^{-\bullet}$. In the case of $\mathbf{Ir}\text{-}\mathbf{OMe}^+$, further irradiation resulted in substantial spectral changes accompanied by decreases of absorbance at 529 nm, a result showing sharp contrast to little spectral change in the case of $\mathbf{Ir}\text{-}^t\mathbf{Bu}^+$.

These observations demonstrate that $[\mathbf{Ir}\text{-}^t\mathbf{Bu}^+]^{-\bullet}$ is stable under visible-light irradiation, whereas $[\mathbf{Ir}\text{-}\mathbf{OMe}^+]^{-\bullet}$ undergo photochemical changes. The different photochemical behavior of $[\mathbf{Ir}\text{-}\mathbf{X}^+]^{-\bullet}$ should have a possible relationship with net chemical

DOI: 10.1021/acs.inorgchem.7b01963
Inorg. Chem. XXXX, XXX, XXX−XXX

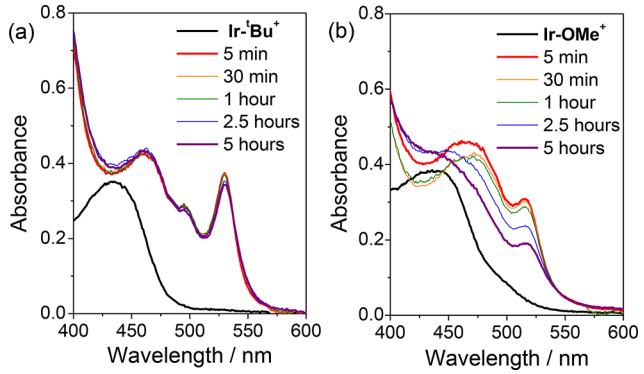

Figure 9. Changes of absorption spectra for **Ir-^{t}Bu$^+$** (a) and **Ir-OMe$^+$** (b) following irradiation time for Ar-saturated DMF solution containing 0.05 mM **Ir-X$^+$** and 0.25 mM BIH; LED irradiation at greater than 400 nm.

stability of PS during the photosensitized CO_2 reduction. Figure 10 shows absorption spectra after the photosensitized

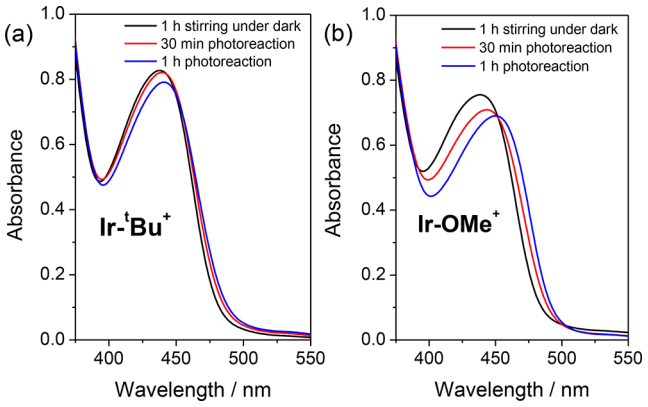

Figure 10. Absorption spectra of **Ir-^{t}Bu$^+$** (a) and **Ir-OMe$^+$** (b) after stirring for 1 h in the dark (black line) and after photosensitized CO_2 reduction for 30 min (red line) and for 1 h (blue line); 3 mL of CO_2-saturated DMF/H_2O mixture solution (2.5 vol % water) of 1 mM **Ir-X$^+$**, 10 mg of TiO_2/ReC(0.1 μmol) particles, and 0.1 M BIH.

CO_2 reduction by the **Ir-X$^+$**−TiO_2/ReC binary systems for 30 min and for 1 h compared with those after stirring of the solutions in the dark for 1 h; the spectra were taken by 10-fold dilution of the solutions separated by centrifugation of the irradiated samples. In the case of **Ir-OMe$^+$**, significant spectral changes occurred during the photosensitized CO_2 reduction, whereas **Ir-^{t}Bu$^+$** was relatively stable. In the case of $Ru(bpy)_3^{2+}$, still faster spectral changes occurred during the photosensitized CO_2 reduction (Figure S22), a result in line with the early appearance of leveling-off behavior of the photosensitized CO_2 reduction. The long-term photosensitization capability of **Ir-^{t}Bu$^+$** compared with **Ir-OMe$^+$** as well as with $Ru(bpy)_3^{2+}$ is mainly attributable to the photochemical stability of [**Ir-^{t}Bu$^+$**]$^{-\bullet}$. Probably, on the one hand, the very bulky and chemically stable ^{t}Bu substituents would block [**Ir-^{t}Bu$^+$**]$^{-\bullet}$ against unwanted chemical changes during the photosensitization cycle. In the case of **Ir-OMe$^+$**, on the other hand, the strong electron-donating effect of the OMe substituent would be divergent; the localization of the odd electron of PS$^{-\bullet}$ on the btp ligand would help the electron injection into TiO_2 but enhance the chemical reactivity of PS$^{-\bullet}$.

Finally, it is of significance to note that the present photosensitized reactions gave formic acid in small, but not negligible, amounts in contrast to the lack of HCOOH formation in the CO_2 reduction by the ternary system (Dye/TiO_2/ReC). Figure S23 shows plots for the formation of CO and HCOOH versus irradiation time in the [**Ir-^{t}Bu**]$^+$−TiO_2/ReC case, revealing that the formation of HCOOH is not increased with irradiation time from the initial amount in contrast to the continuous increase of CO formation. It appears that the major source of HCOOH formed is not CO_2, because irradiation of [**Ir-^{t}Bu**]$^+$−TiO_2/ReC *under* N_2 in the presence of 2.5% H_2O for 4 h gave (5.4 ± 0.4) μmol of HCOOH, in a significantly greater amount compared to the photoreaction under CO_2 (~1.4 μmol of HCOOH; Table S11). On the one hand, the hydrolysis of DMF appears to be a major consequence of the HCOOH formation occurring under irradiation in the presence of [**Ir-^{t}Bu**]$^+$, because HCOOH was not detected after keeping [**Ir-^{t}Bu**]$^+$−TiO_2/ReC in DMF in the presence of 2.5% H_2O for several hours in the dark. On the other hand, irradiation of a DMF solution containing [**Ir-^{t}Bu**]$^+$, BIH, and 2.5% H_2O for 4 h under either CO_2 or N_2 (i.e., without TiO_2/ReC) gave (2.0 ± 0.1) μmol of HCOOH (Table S11). A possible speculation is that DMF would be photochemically hydrolyzed after electron transfer from BIH to ^{3}[**Ir-^{t}Bu**]$^+$*. However, further investigation was not undertaken, because the HCOOH is not a "product" from CO_2.

CONCLUSIONS

The present investigation reveals that **Ir-X$^+$** (X = OMe, ^{t}Bu, Me, and H) commonly works as effective visible-light photosensitizer for the selective reduction of CO_2 to CO by the TiO_2/ReC binary catalyst that proceeds via electron transfer from BIH to excited-state **Ir-X$^+$** followed by electron injection from [**Ir-X$^+$**]$^{-\bullet}$ to TiO_2/ReC. The **Ir-X$^+$**−TiO_2/ReC binary system is more efficient than the Dye/TiO_2/ReC ternary system. While the electron injection from [**Ir-X$^+$**]$^{-\bullet}$ into TiO_2 is supposed to be slightly endergonic unlike exergonic electron injection from excited-state Dye, the higher efficiencies of the binary system is attributed to more efficient light harvesting by **Ir-X$^+$** in solution compared with Dye fixed on TiO_2. The photosensitizers used in the CO_2 reduction based on the binary catalyst show different efficiencies in the order of **Ir-OMe$^+$** > **Ir-^{t}Bu$^+$** ≈ **Ir-Me$^+$** > **Ir-H$^+$** ≫ $Ru(bpy)_3^{2+}$, whereas the long-term stability in the photosensitization cycle is in the order of **Ir-^{t}Bu$^+$** ≈ **Ir-Me$^+$** > **Ir-H$^+$** > **Ir-OMe$^+$** ≫ $Ru(bpy)_3^{2+}$; the **Ir-X$^+$** photosensitizers are considerably more efficient and more robust than $Ru(bpy)_3^{2+}$, a commonly used photosensitizer. The higher photosensitization efficiency of **Ir-OMe$^+$** appears to be attributed to more efficient electron injection from [**Ir-OMe$^+$**]$^{-\bullet}$ into TiO_2 associated with the distribution of odd electron toward btp ligand (relatively high energy level) by the electron-donating OMe substituents. The persistent photosensitization behavior of **Ir-^{t}Bu$^+$** should arise from the photochemical stability of [**Ir-^{t}Bu$^+$**]$^{-\bullet}$, while the photochemical labile property of [**Ir-OMe$^+$**]$^{-\bullet}$ and [$Ru(bpy)_3^{2+}$]$^{-\bullet}$ leads to the leveling-off behavior in the photosensitized CO_2 reduction. The present investigation proves that **Ir-X$^+$** can work in solution as effective and robust photosensitizer for the CO_2 reduction based on the TiO_2/ReC binary catalyst and implies that the structure−reactivity relationships explored in this work might give a strategic basis for molecular design of Ir-complex-based photosensitizers directing to the construction of efficient and persistent CO_2 reduction systems.

DOI: 10.1021/acs.inorgchem.7b01963
Inorg. Chem. XXXX, XXX, XXX−XXX

■ ASSOCIATED CONTENT

Supporting Information

The Supporting Information is available free of charge on the ACS Publications website at DOI: 10.1021/acs.inorgchem.7b01963.

Results of ^{1}H and ^{13}C NMR spectroscopic data for **Ir-CN**$^{+}$, photophysical (UV−vis absorption and photoluminescence spectra) data, electrochemical data (cyclic voltammogram) of samples, ^{13}C isotopic labeled CO_2 NMR/GC-MS experiments, and plots of CO formation versus time for hybrid catalysts (PDF)

Accession Codes

CCDC 1481192 and 1510579 contain the supplementary crystallographic data for this paper. These data can be obtained free of charge via www.ccdc.cam.ac.uk/data_request/cif, or by emailing data_request@ccdc.cam.ac.uk, or by contacting The Cambridge Crystallographic Data Centre, 12 Union Road, Cambridge CB2 1EZ, UK; fax: +44 1223 336033.

■ AUTHOR INFORMATION

Corresponding Authors

*E-mail: hjson@korea.ac.kr. (H.-J.S.)
*E-mail: jjpac@korea.ac.kr. (C.P.)
*E-mail: sangok@korea.ac.kr. (S.-O.K.)

ORCID

Dae Won Cho: 0000-0002-4785-069X
Ho-Jin Son: 0000-0003-2069-1235
Sang Ook Kang: 0000-0002-3911-7818

Notes

The authors declare no competing financial interest.

■ ACKNOWLEDGMENTS

This work was supported by Basic Science Research Program through the National Research Foundation of Korea (NRF) funded by the Ministry of Education (NRF-2014R1A6A1030732), the Functional Districts of the Science Belt support program, Ministry of Science, ICT and Future Planning (2015K000287), and the Basic Science Research Program through the NRF funded by the Ministry of Education (NRF-2016R1D1A3B03934670 and NRF-2016R1D1A3B03936414).

■ REFERENCES

(1) BP statistical Review of World Energy June 2016, Carbon dioxide emissions http://www.bp.com/content/dam/bp/pdf/energy-economics/statistical-review-2016/bp-statistical-review-of-world-energy-2016-full-report.pdf.

(2) Aresta, M.; Dibenedetto, A.; Angelini, A. Catalysis for the Valorization of Exhaust Carbon: from CO_2 to Chemicals, Materials, and Fuels. Technological Use of CO_2. *Chem. Rev.* **2014**, *114*, 1709−1742.

(3) Kondratenko, E. V.; Mul, G.; Baltrusaitis, J.; Larrazabal, G. O.; Perez-Ramirez, J. Status and perspectives of CO_2 conversion into fuels and chemicals by catalytic, photocatalytic and electrocatalytic processes. *Energy Environ. Sci.* **2013**, *6*, 3112−3135.

(4) Markewitz, P.; Kuckshinrichs, W.; Leitner, W.; Linssen, J.; Zapp, P.; Bongartz, R.; Schreiber, A.; Mueller, T. E. Worldwide innovations in the development of carbon capture technologies and the utilization of CO_2. *Energy Environ. Sci.* **2012**, *5*, 7281−7305.

(5) Morris, A. J.; Meyer, G. J.; Fujita, E. Molecular Approaches to the Photocatalytic Reduction of Carbon Dioxide for Solar Fuels. *Acc. Chem. Res.* **2009**, *42*, 1983−1994.

(6) Yui, T.; Tamaki, Y.; Sekizawa, K.; Ishitani, O. Photocatalytic Reduction of CO_2: From Molecules to Semiconductors. *Top. Curr. Chem.* **2011**, *303*, 151−184.

(7) Alibabai, L.; Luo, H.; House, R. L.; Hoertz, P. G.; Meyer, T. J.; et al. Applications of metal oxide materials in dye sensitized photoelectrosynthesis cells for making solar fuels: let the molecules do the work. *J. Mater. Chem. A* **2013**, *1*, 4133−4145.

(8) Hawecker, J.; Lehn, J.-M.; Ziessel, R. Efficient Photochemical Reduction of CO_2 to CO by Visible Light Irradiation of Systems containing $Re(bipy)(CO)_3X$ or $Ru(bipy)_3^{2+}$−Co^{2+} Combinations as Homogeneous Catalysts. *J. Chem. Soc., Chem. Commun.* **1983**, *9*, 536−538.

(9) Hawecker, J.; Lehn, J.-M.; Ziessel, R. Photochemical and Electrochemical Reduction of Carbon Dioxide to Carbon Monoxide Mediated by (2,2′-Bipyridine)tricarbonylchlororhenium (I) and Related Complexes as Homogeneous Catalysts. *Helv. Chim. Acta* **1986**, *69*, 1990−2012.

(10) Yamazaki, Y.; Takeda, H.; Ishitani, O. Photocatalytic reduction of CO_2 using metal complexes. *J. Photochem. Photobiol., C* **2015**, *25*, 106−137.

(11) Bonin, J.; Maurin, A.; Robert, M. Molecular catalysis of the electrochemical and photochemical reduction of CO_2 with Fe and Co metal based complexes. Recent advances. *Coord. Chem. Rev.* **2017**, *334*, 184−198.

(12) Takeda, H.; Cometto, C.; Ishitani, O.; Robert, M. Electrons, Photons, Protons and Earth-Abundant Metal Complexes for Molecular Catalysis of CO_2 Reduction. *ACS Catal.* **2017**, *7*, 70−88.

(13) Tamaki, Y.; Ishitani, O. Supramolecular Photocatalysts for the Reduction of CO_2. *ACS Catal.* **2017**, *7*, 3394−3409.

(14) Elgrishi, N.; Chambers, M. B.; Wang, X.; Fontecave, M. Molecular polypyridine-based metal complexes as catalysts for the reduction of CO_2. *Chem. Soc. Rev.* **2017**, *46*, 761−796.

(15) Willkomm, J.; Orchard, K. L.; Reynal, A.; Pastor, E.; Durrant, J. R.; Reisner, E. Dye-sensitized semiconductors modified with molecular catalysts for light-driven H_2 production. *Chem. Soc. Rev.* **2016**, *45*, 9−23.

(16) Woolerton, T. W.; Sheard, S.; Reisner, E.; Pierce, E.; Ragsdale, S. W.; Armstrong, F. A. Efficient and Clean Photoreduction of CO_2 to CO by Enzyme-Modified TiO_2 Nanoparticles Using Visible Light. *J. Am. Chem. Soc.* **2010**, *132*, 2132−2133.

(17) Windle, C. D.; Pastor, E.; Reynal, A.; Whitwood, A. C.; Vaynzof, Y.; Durrant, J. R.; Perutz, R. N.; Reisner, E. Improving the Photocatalytic Reduction of CO_2 to CO through Immobilisation of a Molecular Re Catalyst on TiO_2. *Chem. - Eur. J.* **2015**, *21*, 3746−3754.

(18) Sato, S.; Arai, T.; Morikawa, T.; Uemura, K.; Suzuki, T. M.; Tanaka, H.; Kajino, T. Selective CO_2 Conversion to Formate Conjugated with H_2O Oxidation Utilizing Semiconductor/Complex Hybrid Photocatalysts. *J. Am. Chem. Soc.* **2011**, *133*, 15240−15243.

(19) Kuriki, R.; Sekizawa, K.; Ishitani, O.; Maeda, K. Visible-Light-Driven CO_2 Reduction with Carbon Nitride: Enhancing the Activity of Ruthenium Catalysts. *Angew. Chem., Int. Ed.* **2015**, *54*, 2406−2409.

(20) Won, D.-I.; Lee, J.-S.; Ji, J.-M.; Jung, W.-J.; Son, H.-J.; Pac, C.; Kang, S. O. Highly Robust Hybrid Photocatalyst for Carbon Dioxide Reduction: Tuning and Optimization of Catalytic Activities of Dye/TiO_2/Re(I) Organic−Inorganic Ternary Systems. *J. Am. Chem. Soc.* **2015**, *137*, 13679−13690.

(21) Ha, E. G.; Chang, J.-A.; Byun, S.-M.; Pac, C.; Jang, D.-M.; Park, J.; Kang, S. O. High-turnover visible-light photoreduction of CO_2 by a Re(I) complex stabilized on dye-sensitized TiO_2. *Chem. Commun.* **2014**, *50*, 4462−4464.

(22) Lee, J.-S.; Won, D.-I.; Jung, W.-J.; Son, H.-J.; Pac, C.; Kang, S. O. Widely Controllable Syngas Production by a Dye-Sensitized TiO_2 Hybrid System with Re^{I} and Co^{III} Catalysts under Visible-Light Irradiation. *Angew. Chem., Int. Ed.* **2017**, *56*, 976−980.

(23) Won, D.-I.; Lee, J.-S.; Cheong, H.-Y.; Cho, M.; Jung, W.-J.; Son, H.-J.; Pac, C.; Kang, S. O. Organic−inorganic hybrid photocatalyst for carbon dioxide reduction. *Faraday Discuss.* **2017**, *198*, 337−351.

(24) Borgarello, E.; Kiwi, J.; Pelizzetti, E.; Visca, M.; Grätzel, M. Photochemical cleavage of water by photocatalysis. *Nature* **1981**, *289*, 158−160.

(25) Abdellah, M.; El-Zohry, A. M.; Antila, L. J.; Windle, C. D.; Reisner, E.; Hammarström, L. Time-Resolved IR Spectroscopy Reveals a Mechanism with TiO_2 as a Reversible Electron Acceptor in a TiO_2−

DOI: 10.1021/acs.inorgchem.7b01963
Inorg. Chem. XXXX, XXX, XXX−XXX

Re Catalyst System for CO_2 Photoreduction. *J. Am. Chem. Soc.* **2017**, *139*, 1226−1232.
(26) Amesta, R.; Amesta, S. C. *Photocatalysis Principles and Applications;* CRC Press: Taylor & Francis Group, 2016.
(27) Lowry, M. S.; Hudson, W. R.; Pascal, R. A., Jr.; Bernhard, S. Accelerated Luminophore Discovery through Combinatorial Synthesis. *J. Am. Chem. Soc.* **2004**, *126*, 14129−14135.
(28) Zhang, P.; Wang, M.; Na, Y.; Li, X.; Jiang, Y.; Sun, L. Homogeneous photocatalytic production of hydrogen from water by a bioinspired $[Fe_2S_2]$ catalyst with high turnover numbers. *Dalton Trans.* **2010**, *39*, 1204−1206.
(29) Cline, E. D.; Adamson, S. E.; Bernhard, S. Homogeneous Catalytic System for Photoinduced Hydrogen Production Utilizing Iridium and Rhodium Complexes. *Inorg. Chem.* **2008**, *47*, 10378−10388.
(30) Tinker, L. L.; McDaniel, N. D.; Curtin, P. N.; Smith, C. K.; Ireland, M. J.; Bernhard, S. Visible light induced catalytic water reduction without an electron relay. *Chem. - Eur. J.* **2007**, *13*, 8726−8732.
(31) Goldsmith, J. I.; Hudson, W. R.; Lowry, M. S.; Anderson, T. H.; Bernhard, S. Discovery and High-Throughput Screening of Heteroleptic Iridium Complexes for Photoinduced Hydrogen Production. *J. Am. Chem. Soc.* **2005**, *127*, 7502−7510.
(32) Whang, D. R.; Sakai, K.; Park, S. Y. Highly Efficient Photocatalytic Water Reduction with Robust Iridium(III) Photosensitizers Containing Arylsilyl Substituents. *Angew. Chem., Int. Ed.* **2013**, *52*, 11612−11615.
(33) Rosas-Hernández, A.; Junge, H.; Beller, M. Photochemical reduction of carbon dioxide to formic acid using ruthenium(II)-based catalysts and visible light. *ChemCatChem* **2015**, *7*, 3316−3321.
(34) Bonin, J.; Robert, M.; Routier, M. Selective and efficient photocatalytic CO_2 reduction to CO using visible light and an iron-based homogeneous catalyst. *J. Am. Chem. Soc.* **2014**, *136*, 16768−16771.
(35) Thoi, V. S.; Kornienko, N.; Margarit, C. G.; Yang, P.; Chang, C. J. Visible-light photoredox catalysis: selective carbon dioxide to carbon monoxide by a nickel *N*-heterocyclic carbene-isoquinoline complex. *J. Am. Chem. Soc.* **2013**, *135*, 14413−14424.
(36) Kuramochi, Y.; Ishitani, O. Iridium(III) 1-Phenylisoquinoline Complexes as a Photosensitizer for Photocatalytic CO_2 Reduction: A Mixed System with a Re(I) Catalyst and a Supramolecular Photocatalyst. *Inorg. Chem.* **2016**, *55*, 5702−5709.
(37) Takizawa, S.-Y.; Shimada, K.; Sato, Y.; Murata, S. Controlling the Excited State and Photosensitizing Property of a 2-(2-Pyridyl)benzo[*b*]thiophene-Based Cationic Iridium Complex through Simple Chemical Modification. *Inorg. Chem.* **2014**, *53*, 2983−2995.
(38) Lee, S.-H.; Park, Y.; Wee, K.-R.; Son, H.-J.; Cho, D. W.; Pac, C.; Choi, W.; Kang, S. O. Significance of Hydrophilic Characters of Organic Dyes in Visible-Light Hydrogen Generation Based on TiO_2. *Org. Lett.* **2010**, *12*, 460−463.
(39) BIH synthesis Zhu, X.-Q.; Zhang, M.-T.; Yu, A.; Wang, C.-H.; Cheng, J.-P. Hydride, Hydrogen Atom, Proton and Electron Transfer Driving Forces of Various Five-membered Heterocyclic Organic Hydrides and Their Reaction Intermediates in Acetonitrile. *J. Am. Chem. Soc.* **2008**, *130*, 2501−2516.
(40) Lamansky, S.; Djurovich, P.; Murphy, D.; Abdel-Razzaq, F.; Lee, H.-E.; Adachi, C.; Burrows, P. E.; Forrest, S. R.; Thompson, M. E. Highly Phosphorescent Bis-Cyclometalated Iridium Complexes: Synthesis, Photophysical Characterization, and Use in Organic Light Emitting Diodes. *J. Am. Chem. Soc.* **2001**, *123*, 4304−4312.
(41) Duong, A.; Maris, T.; Lebel, O.; Wuest, J. D. Syntheses and Structures of Isomeric Diaminotriazinyl-Substituted 2,2′-Bipyridines and 1,10-Phenanthrolines. *J. Org. Chem.* **2011**, *76*, 1333−1341.
(42) Sheldrick, G. M. *SMART, SAINT*, and *SHELXTL-PLUS* Software Package; Bruker Analytical X-Ray Division: Madison, WI, 2002.
(43) Broomhead, J. A.; Young, C. G.; et al. Tris(2, 2′-bipyridine) ruthenium(II) dichloride hexahydrate. *Inorg. Syntheses* **1990**, *28*, 338−340.
(44) Skórka, Ł.; Filapek, M.; Zur, L.; Małecki, J. G.; Pisarski, W.; Olejnik, M.; Danikiewicz, W.; Krompiec, S. Highly Phosphorescent Cyclometalated Iridium(III) Complexes for Optoelectronic Applications: Fine Tuning of the Emission Wavelength through Ancillary Ligands. *J. Phys. Chem. C* **2016**, *120*, 7284−7294.
(45) Tian, N.; Lenkeit, D.; Pelz, S.; Fischer, L. H.; Escudero, D.; Schiewek, R.; Klink, D.; Schmitz, O. J.; González, L.; Schäferling, M.; Holder, E. Structure−Property Relationship of Red- and Green-Emitting Iridium(III) Complexes with Respect to Their Temperature and Oxygen Sensitivity. *Eur. J. Inorg. Chem.* **2010**, *2010*, 4875−4885.
(46) Lalevée, J.; Dumur, F.; Mayer, C. R.; Gigmes, D.; Nasr, G.; Tehfe, M.-A.; Telitel, S.; Morlet-Savary, F.; Graff, B.; Fouassier, J. P. Photopolymerization of *N*-Vinylcarbazole Using Visible-Light Harvesting Iridium Complexes as Photoinitiators. *Macromolecules* **2012**, *45*, 4134−4141.
(47) Sajoto, T.; Djurovich, P. I.; Tamayo, A. B.; Oxgaard, J.; Goddard, W. A.; Thompson, M. E. Temperature Dependence of Blue Phosphorescent Cyclometalated Ir(III) Complexes. *J. Am. Chem. Soc.* **2009**, *131*, 9813−9822.
(48) Caspar, J. V.; Meyer, T. J. Photochemistry of $Ru(bpy)_3^{2+}$. Solvent Effects. *J. Am. Chem. Soc.* **1983**, *105*, 5583−5590.
(49) Hay, P. J. Theoretical Studies of the Ground and Excited Electronic States in Cyclometalated Phenylpyridine Ir(III) Complexes Using Density Functional Theory. *J. Phys. Chem. A* **2002**, *106*, 1634−1641.
(50) Naab, B. D.; Guo, S.; Olthof, S.; Evans, E. G. B.; Wei, P.; Millhauser, G. L.; Kahn, A.; Barlow, S.; Marder, S. R.; Bao, Z. Mechanistic Study on the Solution-Phase n-Doping of 1,3-Dimethyl- 2-aryl-2,3-dihydro-1*H*-benzoimidazole Derivatives. *J. Am. Chem. Soc.* **2013**, *135*, 15018−15025.
(51) Tamaki, Y.; Koike, K.; Morimoto, T.; Yamazaki, Y.; Ishitani, O. Red-Light-Driven Photocatalytic Reduction of CO_2 using Os(II)−Re(I) Supramolecular Complexes. *Inorg. Chem.* **2013**, *52*, 11902−11909.
(52) Kuramochi, Y.; Ishitani, O. Iridium(III) 1-Phenylisoquinoline Complexes as a Photosensitizer for Photocatalytic CO_2 Reduction: A Mixed System with a Re(I) Catalyst and a Supramolecular Photocatalyst. *Inorg. Chem.* **2016**, *55*, 5702−5709.
(53) Yamazaki, Y.; Umemoto, A.; Ishitani, O. Photochemical Hydrogenation of π-Conjugated Bridging Ligands in Photofunctional Multinuclear Complexes. *Inorg. Chem.* **2016**, *55*, 11110−11124.
(54) Ohkubo, K.; Kotani, H.; Shao, J.; Ou, Z.; Kadish, K. M.; Li, G.; Pandey, R. K.; Fujitsuka, M.; Ito, O.; Imahori, H.; Fukuzumi, S. Production of an ultra-long-lived charge-separated state in a zinc chlorin−C_{60} dyad by one-step photoinduced electron transfer. *Angew. Chem., Int. Ed.* **2004**, *43*, 853−856.
(55) Imahori, H.; Guldi, D. M.; Tamaki, K.; Yoshida, Y.; Luo, C.; Sakata, Y.; Fukuzumi, S. Charge Separation in a Novel Artificial Photosynthetic Reaction Center Lives 380 ms. *J. Am. Chem. Soc.* **2001**, *123*, 6617−6628.
(56) Fukuzumi, S.; Ohkubo, K.; Suenobu, T. Long-Lived Charge Separation and Applications in Artificial Photosynthesis. *Acc. Chem. Res.* **2014**, *47*, 1455−1464.
(57) Smieja, J. M.; Kubiak, C. P. Re(bipy-tBu)$(CO)_3$Cl-improved Catalytic Activity for Reduction of Carbon Dioxide: IR-Spectroelectrochemical and Mechanistic Studies. *Inorg. Chem.* **2010**, *49*, 9283−9289.
(58) Sullivan, B. P.; Bolinger, C. M.; Conrad, D.; Vining, W. J.; Meyer, T. J. One- and Two-electron Pathways in the Electrocatalytic Reduction of CO_2 by *fac*-Re(bpy)$(CO)_3$Cl (bpy = 2,2′-bipyridine). *J. Chem. Soc., Chem. Commun.* **1985**, *20*, 1414−1416.
(59) Takeda, H.; Koike, K.; Inoue, H.; Ishitani, O. Development of an Efficient Photocatalytic System for CO_2 Reduction Using Rhenium(I) Complexes Based on Mechanistic Studies. *J. Am. Chem. Soc.* **2008**, *130*, 2023−2031.
(60) Koike, K.; Hori, H.; Ishizuka, M.; Westwell, J. R.; Takeuchi, K.; Ibusuki, T.; Enjouji, K.; Konno, H.; Sakamoto, K.; Ishitani, O. Key Process of the Photocatalytic Reduction of CO_2 Using $[Re(4,4'\text{-}X_2\text{-}bipyridine)(CO)_3PR_3]^+$ (X = CH_3, H, CF_3; PR_3 = Phosphorus Ligands): Dark Reaction of the One-Electron-Reduced Complexes with CO_2. *Organometallics* **1997**, *16*, 5724−5729.

DOI: 10.1021/acs.inorgchem.7b01963
Inorg. Chem. XXXX, XXX, XXX−XXX

(61) Hori, H.; Johnson, F. P. A.; Koike, K.; Takeuchi, K.; Ibusuki, T.; Ishitani, O. Photochemistry of $[Re(bipy)(CO)_3(PPh_3)]^+$ (bipy = 2,2′-bipyridine) in the presence of triethanolamine associated with photoreductive fixation of carbon dioxide: participation of a chain reaction mechanism. *J. Chem. Soc., Dalton Trans.* **1997**, *6*, 1019−1024.
(62) Morimoto, T.; Nakajima, T.; Sawa, S.; Nakanishi, R.; Imori, D.; Ishitani, O. CO_2 Capture by a Rhenium(I) Complex with the Aid of Triethanolamine. *J. Am. Chem. Soc.* **2013**, *135*, 16825−16828.
(63) Hori, H.; Ishihara, J.; Koike, K.; Takeuchi, K.; Ibusuki, T.; Ishitani, O. Photocatalytic reduction of carbon dioxide using $[fac$-$Re(bpy)(CO)_3(4\text{-}Xpy)]^+$ (Xpy = pyridine derivatives). *J. Photochem. Photobiol., A* **1999**, *120*, 119−124.
(64) Takeda, H.; Koike, K.; Inoue, H.; Ishitani, O. Development of an Efficient Photocatalytic System for CO_2 Reduction Using Rhenium(I) Complexes Based on Mechanistic Studies. *J. Am. Chem. Soc.* **2008**, *130*, 2023−2031.
(65) Hayashi, Y.; Kita, S.; Brunschwig, B. S.; Fujita, E. Involvement of a Binuclear Species with the Re−C(O)O−Re Moiety in CO_2 Reduction Catalyzed by Tricarbonyl Rhenium(I) Complexes with Diimine Ligands: Strikingly Slow Formation of the Re−Re and Re−C(O)O−Re Species from $Re(dmb)(CO)_3S$ (dmb = 4,4′-Dimethyl-2,2′-bipyridine, S = Solvent). *J. Am. Chem. Soc.* **2003**, *125*, 11976−11987.
(66) Reynal, A.; Lakadamyali, F.; Gross, M. A.; Reisner, E.; Durrant, J. R. Parameters affecting electron transfer dynamics from semiconductors to molecular catalysts for the photochemical reduction of protons. *Energy Environ. Sci.* **2013**, *6*, 3291−3300.

DOI: 10.1021/acs.inorgchem.7b01963
Inorg. Chem. XXXX, XXX, XXX−XXX